PCCP

ROYAL SOCIETY OF CHEMISTRY

PERSPECTIVE

Published on 23 June 2025
Licence and permissions

Cite this: *Phys. Chem. Chem. Phys.*, 2025, **27**, 14718

New perspectives addressing application challenges in concentration cells

Zeshuo Meng,*[ab] Runlin Zhang,[ab] Haoteng Sun,*[c] Jingchen Zhang,[e] Xiliang Gong[f] and Zhengyan Du*[d]

Received 22nd May 2025,
Accepted 20th June 2025

DOI: 10.1039/d5cp01934f

rsc.li/pccp

Due to the outstanding characteristics of concentration batteries, they are considered a key technology that should provide a future breakthrough in the energy sector. However, the lack of strategic guidance from engineering and scientific theories has posed significant challenges to the engineering development process of these novel devices. This paper, based on the new technical theoretical perspective of the diffusion flux-driving force equation, proposes a new degree of freedom for optimizing the realization of physical devices to enhance their practical usability. Subsequently, we categorized and summarized concentration batteries, deriving the theoretical electromotive force (EMF) of various devices based on their operational characteristics. By combining multiple numerical simulations of the models, we confirmed that these devices possess high energy storage activity and stability. Additionally, based on this theoretical framework, we identified key directions for breakthroughs necessary for the realization of concentration batteries in the future. By integrating the planning of theoretical development with practical realities and addressing developmental issues from a more cutting-edge perspective, we will lay a solid foundation for the rapid realization of the large-scale and personalized application of the next generation of new energy storage devices.

1. Introduction

In recent years, energy issues have become increasingly prominent worldwide. With the continuous growth of the population and rapid economic development, the demand for energy has surged dramatically.[1–3] However, traditional energy resources are limited and non-renewable, and the carbon emissions resulting from the use of fossil fuels have a severe impact on global climate change.[4–6] In this context, finding sustainable clean energy solutions has become particularly important.[7–9] Chemical power sources, as an important technology for energy conversion and storage, play an extremely significant role in alleviating the current energy crisis.[8,10,11] However, concentration cells, as one of the classic representatives of chemical power sources, have often been overlooked due to various scientific and technological reasons, resulting in relatively slow progress in their practical applications.[12–14] Unfortunately, this neglect is misguided and significantly hinders the development of new solutions to energy problems.

Concentration cells are devices that convert the concentration gradient in a solution into electrical energy. They drive the flow of electrons by utilizing the ionic flux generated from the concentration difference, thereby achieving energy conversion.[15,16] Compared to traditional battery technologies, concentration cells offer numerous advantages such as low cost, environmental friendliness, and higher energy density.[17–19] The concentration cell is regarded as a critical technology that needs to be advanced in the future of the energy sector, with extremely broad application prospects.[20–23] In recent years, some outstanding studies have been reported on novel energy storage devices based on the theory of concentration cells. These technologies have achieved new breakthroughs in addressing certain key issues, providing new technical perspectives for the design of such devices.[24–29] However, despite the great potential of concentration cells, they still face several challenges and issues that hinder their practical development and large-scale application.[30–32] Firstly, the design and fabrication of concentration cells are relatively complex processes. To achieve efficient energy conversion, it is necessary to precisely control the internal circuit structure, optimize the characteristics of the electrolyte, and select appropriate

[a] *School of Nano Technology and Nano Bionics, University of Science and Technology of China, Hefei 230026, China. E-mail: mengzs21@mails.jlu.edu.cn*
[b] *i-lab, Nano-X Vacuum Interconnected Workstation, Suzhou Institute of Nano-Tech and Nano-Bionics, Chinese Academy of Sciences, Suzhou 215123, China*
[c] *Department of Chemistry, Brown University, Rhode Island 02912, USA. E-mail: haoteng_sun@brown.edu*
[d] *Chinese Academy of Sciences Key Laboratory of Urban Pollutant Conversion, Department of Environmental Science and Engineering, University of Science and Technology of China, Hefei 230026, China. E-mail: zhengyandu@mail.ustc.edu.cn*
[e] *Institute for Physical Science and Technology, University of Maryland, College Park, MD, 20742, USA*
[f] *Department of Chemistry and Biochemistry, University of Maryland, College Park, MD, 20742, USA*

transport ions, among other factors. The interactions between these factors still require in-depth research. Secondly, the stability of concentration cells is another critical issue that cannot be overlooked. The challenges of imbalance caused by ion transport and changes in solution concentration affecting electrode materials and membranes need to be addressed. Additionally, concentration cells still face the drawback of insufficient electromotive force in practical applications, which limits the efficiency and reliability of their power output. This urgently requires a collaborative solution through internal optimization and external design of the battery. Therefore, from a holistic perspective, exploring and addressing the challenging issues of concentration cells through new theoretical approaches will have decisive significance for the development of novel energy storage devices.

In this paper, we propose a new degree of freedom for regulating ion mobility based on the new technical theoretical perspective of the diffusion flux-driving force equation, aimed at enhancing the theoretical electromotive force (EMF) of individual units and accelerating the engineering process. Next, we classify concentration batteries based on their fundamental working principles and operational characteristics, and derive the theoretical EMF of various devices to predict their potential application value. To validate the practical working capabilities of these theoretical models, we conducted tests on various concentration batteries using COMSOL multiphysics simulations, and the results indicated that these batteries possess high energy storage activity and stability. Additionally, based on the specific technical parameters provided by the theoretical framework, we present a series of future-oriented recommendations, including the manufacture of highly integrated micro concentration battery devices, the design of bidirectional diffusion ion systems, and the optimization of the viscosity of the electrolytes on both sides to achieve multi-faceted enhancements of the theoretical EMF of concentration batteries. We also recommend hardware upgrades for the concentration battery systems, the development of adaptive advanced theoretical simulations to accurately assess the lifecycle parameters of the batteries, and the construction of new *in situ* testing devices to reveal the dynamic changes at the interface under operational conditions. We firmly believe that by relying on a new technological theoretical perspective and combining it with specific practical situations, top-level design and intelligent manufacturing of the next generation of concentration battery systems will provide profound guidance from a strategic and holistic viewpoint.

2. Computational section

This study uses a one-dimensional (1D) model to simulate the ion transport process because the main concentration gradient is perpendicular to the membrane interface (x-direction), and the symmetry of the electrodes allows the gradients in the y and z directions to be neglected. The calculation method in this paper is based on COMSOL phase-field simulations. In the geometric space of this model, the electrolyte region ranges from 0 to 100 μm, while the membrane region lies between 100 and 125 nm. All experiments were conducted at room temperature, 293.15 K. C_{A_0}/C_{B_0} represents the low-concentration end, assumed to correspond to a_1 in the original manuscript, and all simulations were conducted under the premise that $a_1 < a_2$. Each set of data includes three charts: (1) the electrolyte potential difference measured for different a_1 values (150, 50, and 500) under the blocking concentration c_{lm} = 1000 mol m^{-3}; (2) the potential difference measured for different blocking concentrations c_{lm} (0, 20, and 100) when a_1 is 150 mol m^{-3}; and (3) the electrochemical potential of the dominant ion under different a_1 conditions.

The model is based on a three-dimensional current distribution and utilizes the Nernst–Planck–Poisson (NPP) method. Under the high ion flux conditions considered in this model, it can be neglected. The NPP equation combines the Nernst–Planck equation and the Poisson equation, allowing for the simultaneous consideration of both charge and mass conservation. The Nernst–Planck equation describes ion migration, diffusion, and convection, and its expression is as follows:

$$J_i = -D_i \frac{\mathrm{d}}{\mathrm{d}x} c_i - \frac{Z_i D_i F}{RT} c_i \frac{\mathrm{d}}{\mathrm{d}x} \Phi + c_i v \tag{1}$$

where J_i is the flux of ion i, D_i is the diffusion coefficient of ion i, c_i is the concentration of ion i, z_i is the charge number of ion i, F is the Faraday constant, R is the gas constant, T is the absolute temperature, ϕ is the electric potential, and v is the convection velocity.

For ion i, the form of its mass conservation equation is:

$$\frac{\partial c_i}{\partial t} + \nabla \cdot J_i = 0 \tag{2}$$

The Poisson equation describes the relationship between the electric potential ϕ and the charge density ρ:

$$\nabla^2 \Phi = -\frac{\rho}{\epsilon} \tag{3}$$

where ρ is the charge density, which equals the sum of the charges of all ions:

$$\rho = \sum_i Z_i F c_i \tag{4}$$

The blocking concentration c_{lm} in the model depends on the Donnan exclusion concentration. Under Donnan equilibrium conditions, the ion concentrations inside and outside the membrane follow the relationship:

$$\frac{c_{m,i}\gamma_{m,i}}{c_{s,i}\gamma_{s,i}} = \mathrm{e}^{\frac{z_i F \Delta\psi}{RT}} \tag{5}$$

where $c_{m,i}$ is the concentration of ion i inside the membrane, $c_{s,i}$ is the concentration of ion i in the solution, $\gamma_{m,i}$ is the activity coefficient of ion i in the solution inside the membrane, $\gamma_{s,i}$ is the activity coefficient of ion i in the solution outside the membrane, z_i is the charge number of ion i, F is the Faraday constant, $\Delta\psi$ is the potential difference across the membrane, R is the gas constant, T is the absolute temperature, and C_f is the fixed charge density of the membrane.

The Donnan equilibrium condition provides the following relationship:

$$\Delta\psi = \frac{RT}{z_i F}\sinh^{-1}\left(\frac{C_f}{2\sum_i z_i c_{s,i}}\right) \quad (6)$$

The final general expression for the blocking concentration is:

$$\frac{c_{m,i}\gamma_{m,i}}{c_{s,i}\gamma_{s,i}} = e^{\sinh^{-1}\left(\frac{C_f}{2\sum_i z_i c_{s,i}}\right)} \quad (7)$$

$$c_{m,i} = \frac{c_{s,i}\gamma_{s,i}}{\gamma_{m,i}} e^{\sinh^{-1}\left(\frac{C_f}{2\sum_i z_i c_{s,i}}\right)} \quad (8)$$

We have clearly divided the system into three regions (left electrolyte/membrane/right electrolyte) and defined the boundary conditions based on concentrated solution theory. (1) Electrode boundaries ($x = 0$ and $x = L_3$), ions are impermeable: $J_i \cdot n = 0$, potential boundary conditions: $\phi = \phi_{electrode}$. (2) Electrolyte–membrane interfaces ($x = L_1$ and $x = L_2$), continuity of ion flux: at the left interface: $J_i^L \cdot n = J_i^M \cdot n$. At the right interface: $J_i^M \cdot n = J_i^R \cdot n$.

3. Results and discussion

3.1 The working principle and classification of concentration cells

Energy is one of the most important issues in the development of human society.[33,34] Currently, the majority of global energy demand relies on fossil fuels.[35–37] However, fossil fuels are non-renewable and will eventually be depleted, and their extensive use also leads to serious environmental pollution issues.[38–41] Therefore, researching new types of chemical power sources has become increasingly important.[42,43] As a classic electrochemical cell theoretical model, the concentration cell has seen relatively slow progress in practical development, leading to insufficient research and exploration efforts. Therefore, theoretically investigating the issues in this energy storage system and finding corresponding solutions is crucial for achieving its large-scale application as soon as possible.

The core working process of a concentration cell involves the transfer of substances (including elements or ions) from high concentration to low concentration, accompanied by the conversion of Gibbs free energy into electrical energy.[44–47] Simply put, a concentration cell is able to generate electrical energy because there is a concentration gradient of substances within the cell system.[48,49] This phenomenon of energy exchange relying on concentration gradients is widely observed in nature, such as at river estuaries where there is a significant salinity difference, leading to substantial energy conversion. It has been calculated that the energy resources from global seawater salinity differences amount to 3 billion kilowatts. In light of this, our previous research has thoroughly discussed the relationship between diffusion flux and concentration gradients of substances, and the following expression was derived:[50]

$$J = -\frac{DC}{R}\frac{\partial^2 S}{\partial N \partial x} \quad (9)$$

In this equation, J represents the diffusion flux, D is the diffusion coefficient, C is the molar concentration, N is the number of particles in the system, x is the generalized coordinate related to the mean free path, and S is the ion mixing entropy, representing the degree of ion mixing.

Furthermore, by substituting the diffusion coefficient $D = D_0 e^{\frac{-E_a}{RT}}$ into the diffusion flux-driving force equation, the expanded form of this equation can be obtained:

$$J = -\frac{D_0 C}{R}\frac{\partial^2 S}{\partial N \partial x} e^{\frac{-E_a}{RT}} = -\frac{D_0 C}{R}\frac{\partial^2 S}{\partial N \partial x} e^{\frac{-E_a}{RT}} \quad (10)$$

Here, we can observe that the ion diffusion flux is determined by two coefficients: the linear control coefficient $\frac{\partial^2 S}{\partial N \partial x}$ and the exponential control coefficient $e^{\frac{-E_a}{RT}}$. The linear control coefficient represents the gradient of ion concentration distribution in space, indicating that the influence of the concentration gradient on the diffusion flux is linear. This means that changing the concentration gradient has a relatively smaller effect on the diffusion flux compared to the synchronized adjustment of the exponential control coefficient, thus limiting its impact on the potential. This insight provides new approaches for optimizing the design of concentration cell devices, potentially accelerating the development of new practical devices.

3.2 Theoretical potential derivation and device simulation of various concentration cells

Based on the operational characteristics of concentration cells, they can be divided into two main categories:[49,51,52] electrode concentration cells and electrolyte concentration cells. Electrode concentration cells are driven by the potential difference caused by the difference in the concentration of active materials at the electrodes. This type of concentration cell contains only one electrolyte solution. On the other hand, electrolyte concentration cells are driven by the difference in electrode potential due to the concentration gradient of electrolytes in the cell. These cells contain at least two electrolyte solutions with different concentrations, and the electrode potential is related to the concentration gradient of the electrolyte solution. Therefore, the potential formed by a concentration cell can be calculated according to thermodynamic laws:[53,54]

$$\Delta_r G_M^\theta = -zFE^\theta \quad (11)$$

From the Gibbs free energy equation, it is known that:

$$c = \Delta_r H_M^\theta - T\Delta_r S_M^\theta \quad (12)$$

Substituting eqn (11) into eqn (12) gives:

$$zFE^\theta = -\Delta_r H_M^\theta + T\Delta_r S_M^\theta \quad (13)$$

In this equation, z represents the charge number, F is the Faraday constant, E^θ is the electromotive force, $\Delta_r H_M^\theta$ is the

standard molar enthalpy change, T is the temperature, $\Delta_r G_M^\theta$ is the change in standard molar Gibbs free energy, and $\Delta_r S_M^\theta$ is the standard molar entropy change.

From this, it can be seen that the energy for electrical work in a concentration cell comes from two sources:[55–59] first, the heat effect of the cell reaction, which represents the energy change of the system itself; second, the product of the entropy change and temperature resulting from the interaction between the system and the environment. If $\Delta_r S_M^\theta > 0$, it indicates that the system provides energy to the environment, and the system's energy decreases; if $\Delta_r S_M^\theta < 0$, it means the system absorbs energy from the environment. In concentration cells, although the reaction heat effect $\Delta_r H_M^\theta = 0$, the system's entropy increases due to the spontaneous diffusion of electrolyte ions from high to low concentration ($\Delta_r S_M^\theta > 0$). As the ions diffuse, the system continuously absorbs energy from the environment and converts it into electrical work. Next, we will classify different concentration cell scenarios and conduct theoretical device simulations to confirm their high potential application value.

3.2.1 Electrolyte concentration cell

3.2.1.1 Gas concentration electrode. We constructed the following electrochemical cell to explore the theoretical electromotive force that this cell can generate (Fig. 1a). In this cell, both electrodes are made of Pt, and hydrogen gas (H_2) at 1 atm is supplied to both sides. The two chambers are separated by a membrane, and the electrolyte used is HCl solution. The membrane selectively allows the passage of H^+ and Cl^- ions. The ion activity in the S_1 electrode chamber is a_1, and in the S_2 chamber is a_2, with $a_1 > a_2$. Thus, we have established an electrolyte concentration cell with a gas electrode as its core (Pt/H_2 (1 atm)|H^+, $Cl^-(a_1)$|H^+, $Cl^-(a_2)$|H_2 (1 atm)/Pt′).

Here, the total ion flux (J) is defined as the sum of the fluxes of H^+ and Cl^-:

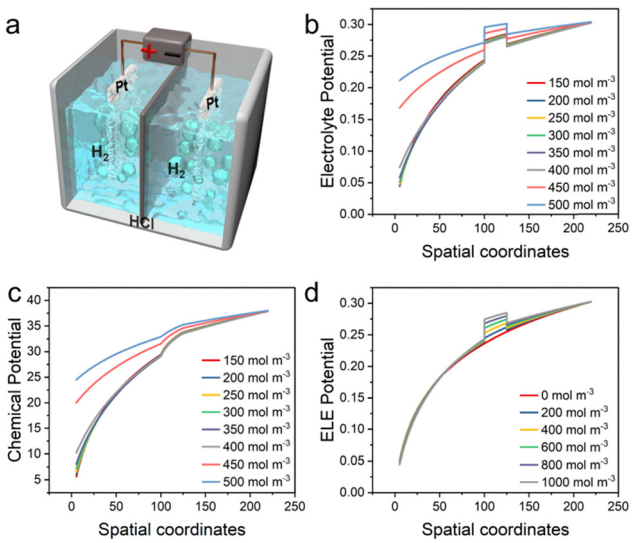

Fig. 1 (a) Schematic diagram of the gas concentration cell device. The curve of (b) electrolyte potential variation, (c) chemical potential, and (d) ELE potential with position in the gas concentration cell device.

$$J = J_{H^+} + J_{Cl^-} \tag{14}$$

Thus, the expressions for the transference numbers are as follows: $t_{H^+} = J_{H^+}/J$, $t_{Cl^-} = J_{Cl^-}/J$ and $t_{H^+} + t_{Cl^-} = 1$. Therefore, we have:

$$t_{H^+} \cdot H_{(S_1)}^{+} + t_{Cl^-} \cdot Cl_{(S_2)}^{-} \leftrightarrow t_{H^+} \cdot H_{(S_2)}^{+} + t_{Cl^-} \cdot Cl_{(S_2)}^{-} \tag{15}$$

Thus, the following equation can be obtained:

$$t_{H^+} \cdot \overline{\mu_{H^+}^{S_1}} + t_{Cl^-} \cdot \overline{\mu_{Cl^-}^{S_2}} = t_{H^+} \cdot \overline{\mu_{H^+}^{S_2}} + t_{Cl^-} \cdot \overline{\mu_{Cl^-}^{S_1}} \tag{16}$$

After rearranging, we obtain:

$$\begin{aligned} &t_{H^+} \cdot \left(\mu_{H^+}^* + RT\ln a_1 + F\varphi_{S_1}\right) + t_{Cl^-} \cdot \left(\mu_{Cl^-}^* + RT\ln a_2 - F\varphi_{S_2}\right) \\ &= t_{H^+} \cdot \left(\mu_{H^+}^* + RT\ln a_2 + F\varphi_{S_2}\right) \\ &+ t_{Cl^-} \cdot \left(\mu_{Cl^-}^* + RT\ln a_1 - F\varphi_{S_1}\right) = t_{H^+} \cdot F \cdot \left(\varphi_{S_2} - \varphi_{S_1}\right) \\ &+ t_{Cl^-} \cdot F \cdot \left(\varphi_{S_2} - \varphi_{S_1}\right) = -t_{H^+} \cdot RT\ln\frac{a_2}{a_1} + t_{Cl^-} \cdot RT\ln\frac{a_2}{a_1} \end{aligned} \tag{17}$$

Thus, we obtain:

$$\begin{aligned} E_J &= \varphi_{S_2} - \varphi_{S_1} = -\frac{t_{H^+} - t_{Cl^-}}{t_{H^+} + t_{Cl^-}} \cdot \frac{RT}{F}\ln\frac{a_2}{a_1} \\ &= -\left(t_{H^+} - t_{Cl^-}\right) \cdot \frac{RT}{F}\ln\frac{a_2}{a_1} = -\frac{RT}{F}\ln\frac{a_2}{a_1} \end{aligned} \tag{18}$$

Therefore, the theoretical electromotive force (EMF) of this concentration cell is:

$$\begin{aligned} E_{cell} &= \frac{RT}{F}\ln\frac{a_2}{a_1} + E_J = \left(1 - t_{H^+} + t_{Cl^-}\right)\frac{RT}{F}\ln\frac{a_2}{a_1} \\ &= 2t_{Cl^-}\frac{RT}{F}\ln\frac{a_1}{a_2} \end{aligned} \tag{19}$$

From the expression for the theoretical EMF, it can be seen that the EMF is proportional to the ionic transference numbers and the activity ratio between the ions in the two chambers. To validate the potential application capabilities of these energy storage devices, we constructed practical models based on the aforementioned theory and conducted phase field simulations in COMSOL. Fig. 1a illustrates a schematic diagram of the gas-phase concentration battery device, where the electrodes on both sides are platinum (Pt), the solution consists of hydrochloric acid (HCl) at different concentrations, and hydrogen gas (H_2) serves as the reactive gas, with the solution separated by a diaphragm. Fig. 1b shows the curve of electrolyte potential as a function of position, with different colors representing different concentrations of the electrolyte solution (ranging from 150 mol m^{-3} to 500 mol m^{-3}). The results indicate that the electrolyte potential increases with position, and a significant potential jump occurs at the diaphragm, highlighting the diaphragm's critical role in regulating ion migration. Notably, as the concentration increases, the value of the electrolyte potential gradually rises, demonstrating the significant impact of concentration gradients on electrolyte potential. Fig. 1c presents the curve of chemical potential as a function of position, showing a trend consistent with that of the electrolyte potential. Fig. 1d displays the curve of ELE potential as

a function of position for different concentrations (ranging from 0 mol m^{-3} to 1000 mol m^{-3}). The results show that the ELE potential increases with position, and the ELE potential curves for different concentrations nearly overlap, indicating that concentration has a minimal effect on the ELE potential. However, the ELE potential also exhibits a jump at the diaphragm, further confirming its crucial role in maintaining the stability of the potential distribution.

Analysis of the above data indicates that both theoretical and simulation results demonstrate significant effects of concentration gradients on electrolyte potential and chemical potential. Specifically, the electrolyte potential and chemical potential increase with concentration, while the ELE potential remains relatively stable, showing that these devices possess both stability and high activity. Furthermore, the potential difference of the hydrogen (H_2) battery is significantly higher than that of other types of batteries, likely due to the high diffusion coefficient of gaseous mass transfer species. In summary, concentration batteries effectively regulate electrolyte potential and chemical potential through concentration gradients, providing an efficient and stable energy conversion pathway.

3.2.1.2 Amalgam concentration electrodes. Following the same approach as above, we inserted two amalgamated sodium electrodes with different concentrations into a Na^+ solution of a certain concentration to construct a concentration cell and conducted an EMF analysis (Fig. 2a) (Na–Hg(a_1)|Na^+(a)|Na–Hg(a_2), ($a_1 > a_2$)). First, we list the overall reaction equation occurring in this cell:

$$\text{Overall reaction: } \mathrm{Na}(a_1) \rightarrow \mathrm{Na}(a_2)$$

For the spontaneous reaction occurring in the concentration cell, the high concentration amalgamated sodium (a_1) is converted into low concentration amalgamated sodium (a_2), resulting in the generation of EMF. Therefore, based on the derived form above, the theoretical electromotive force of this cell can be expressed as:

$$E_{\text{cell}} = -\frac{RT}{F}\ln\frac{a_2}{a_1}$$

To validate the potential value of these devices, we obtained performance parameters through COMSOL simulations. Fig. 2a shows a schematic diagram of the sodium amalgam concentration battery, where the electrodes on both sides are Na–Hg, and the solution contains Na^+ ions at different concentrations, separated by a diaphragm. Fig. 2b displays the curve of electrolyte potential as a function of position. The results indicate that the electrolyte potential increases with position, and a significant potential jump occurs at the diaphragm, demonstrating that the concentration battery generates a potential difference through the concentration gradient, with the diaphragm playing a crucial role in regulating ion migration. Notably, as the concentration increases, the electrolyte potential gradually rises, further confirming the significant impact of the concentration gradient on electrolyte potential. Fig. 2c presents the curve of chemical potential as a function of position, with different colors representing solutions of varying concentrations. The results show that chemical potential increases with position, and there are clear

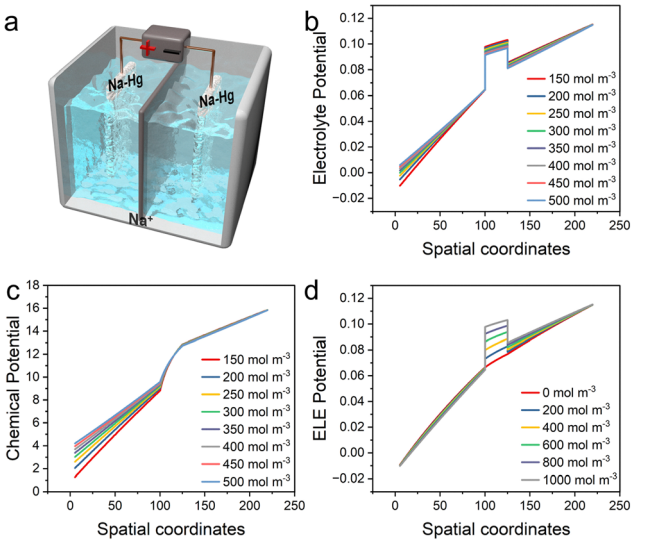

Fig. 2 (a) Schematic diagram of the sodium amalgam concentration cell device. The curve of (b) electrolyte potential variation, (c) chemical potential, and (d) ELE potential with position in the sodium amalgam concentration cell device.

differences in the chemical potential changes at different concentrations, with the curve for higher concentrations significantly exceeding that for lower concentrations. The jump in chemical potential at the diaphragm further validates its role in regulating ion migration, indicating that the high-concentration region provides a stronger energy driving force, thereby optimizing the energy collection efficiency of the battery. Fig. 2d displays the curve of ELE potential as a function of position. The results indicate that the ELE potential increases with the position, and the ELE potential curves for different concentrations nearly overlap, suggesting that concentration has a minimal effect on ELE potential. However, the ELE potential also exhibits a jump at the diaphragm, further confirming the diaphragm's critical role in maintaining the stability of the potential distribution.

3.2.2 Electrode concentration cells

3.2.2.1 Metal concentration cells. The concentration cell constructed with metal electrodes is a classic model. For spontaneous battery reactions, when there is a significant concentration difference, high-concentration electrolyte ions (a_1) will convert to low-concentration electrolyte ions (a_2), thus generating electromotive force. This type of concentration cell is referred to as a cation-reversible concentration cell. Therefore, we discuss this battery model by inserting an Ag electrode into $AgNO_3$ solutions of different concentrations (Ag|$AgNO_3$(a_1)||$AgNO_3$(a_2)|Ag). Therefore, the overall reaction of the concentration cell is:

$$\mathrm{Ag}^+(a_1) \rightarrow \mathrm{Ag}^+(a_2)$$

Based on the above derivation, the electromotive force of this concentration cell is:

$$E_{\text{cell}} = -\frac{RT}{F}\ln\frac{a_2}{a_1}$$

To verify the potential working capability of the silver concentration battery, Fig. 3a presents a theoretical schematic

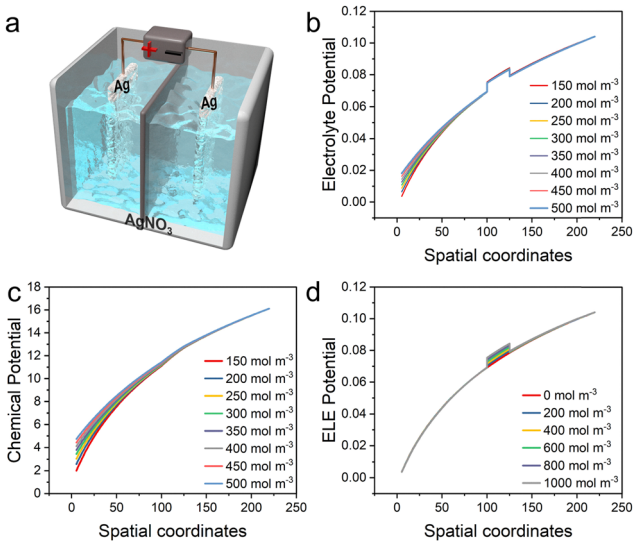

Fig. 3 (a) Schematic diagram of the metallic silver concentration cell device. The curve of (b) electrolyte potential variation, (c) chemical potential, and (d) ELE potential with position in the metallic silver concentration cell device.

diagram. As shown, the electrochemical cell features silver (Ag) electrodes on both sides, with a solution of different concentrations of silver nitrate ($AgNO_3$) separated by a diaphragm, creating two independent solution zones. Fig. 3b–d illustrate the spatial distribution characteristics of the electrolyte potential, chemical potential, and ELE potential based on experimental and simulated results under different concentration conditions. Fig. 3b shows that the electrolyte potential gradually increases with the variation of different concentration gradients, indicating that the electrolyte potential is driven by the concentration gradient and varies at different positions. The chemical potential distribution in Fig. 3c also increases with position, with significant differences in chemical potential changes at different concentrations, reflecting the notable impact of concentration on the distribution of chemical potential. Fig. 3d displays the distribution characteristics of the ELE potential, which indicates that the ELE potential increases with position, and the ELE potential curves at different concentrations nearly overlap, suggesting that concentration has a minimal effect on the ELE potential. These results demonstrate that, driven by the concentration gradient, the electrolyte potential and chemical potential exhibit significant spatial distribution changes, while the ELE potential remains relatively stable. The presence of the diaphragm not only maintains the concentration gradient but also ensures the continuity and stability of the potential distribution.

3.2.2.2 Metal micro-soluble concentration cells. For the concentration cell constructed with metal micro-soluble electrodes, we use Ag and AgCl(s) as the positive and negative electrodes, respectively, inserted into hydrochloric acid (HCl) solutions of different concentrations (Ag, AgCl(s)|HCl(a_1)||HCl(a_2)|AgCl(s), Ag). Therefore, the overall reaction of the concentration cell is:

$$Cl^-(a_1) \rightarrow Cl^-(a_2)$$

When $a_1 > a_2$, the battery reaction occurs spontaneously, and this concentration cell is referred to as an anion-reversible concentration cell. Therefore, the electromotive force of this cell is:

$$E_{cell} = -\frac{RT}{F}\ln\frac{a_2}{a_1}$$

Fig. 4 illustrates the structure of the metal micro-soluble electrode and its spatial distribution based on COMSOL simulations. Fig. 4a presents a schematic diagram of the device, showing that the electrodes on both sides are Ag/AgCl, with the solution consisting of hydrochloric acid (HCl) at different concentrations, separated by a diaphragm. In this system, the working ion for concentration diffusion is Cl^-. Fig. 4b–d display the spatial distribution characteristics of the electrochemical potential, chemical potential, and electrolyte potential based on COMSOL simulations. The simulation results indicate that the side with a higher concentration exhibits a stronger driving force, while the side with a lower concentration tends to be more subdued. The presence of the diaphragm not only maintains the concentration gradient but also ensures the continuity and stability of the potential distribution. Therefore, the metal micro-soluble electrode effectively drives the conversion of electrochemical energy through concentration differences, demonstrating good energy storage potential.

A comprehensive analysis of the above device reveals that for concentration batteries dominated by a single type of ion (such as only Na^+ or Cl^-), higher blocking barriers (for cation dominance) or potential wells (for anion dominance) are more likely to occur. This is due to the lack of compensating effects from oppositely charged ions that maintain electrical neutrality. In concentration batteries dominated solely by Na^+ or Cl^- ions, the migration of ions is influenced by both the electric

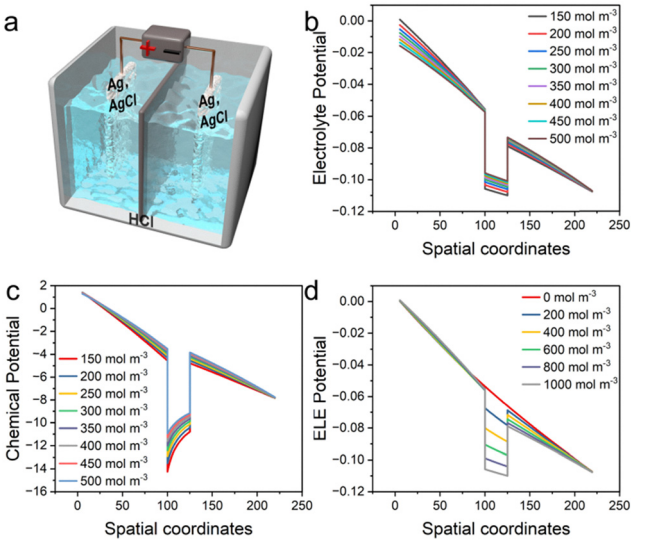

Fig. 4 (a) Schematic diagram of the metal sparingly soluble concentration cell device. The curve of (b) electrolyte potential variation, (c) chemical potential, and (d) ELE potential with position in the metal sparingly soluble concentration cell device.

field and the concentration gradient. To maintain electrical neutrality, the migration of cations leads to the migration of anions and *vice versa*. Without other oppositely charged ions to supplement the neutrality effect, this inter-ionic migration becomes more pronounced, resulting in higher blocking barriers or potential wells.

3.2.2.3 Gas concentration cells. The gas concentration cell is also a classic model of a concentration cell. For example, chlorine gas (Cl_2) is introduced on both the positive and negative electrode sides, while the electrolyte consists of a solution containing different concentrations of Cl^- ($Cl_2(p)|Cl^-(a_1)||Cl^-(a_2)|Cl_2(p)$). The overall reaction of this concentration cell is the same as that in the metal micro-soluble cell:

$$Cl^-(a_1) \rightarrow Cl^-(a_2)$$

Therefore, when $a_1 > a_2$, $E > 0$, this concentration cell is also an anion-reversible concentration cell. Thus, its theoretical electromotive force is:

$$E_{cell} = -\frac{RT}{F}\ln\frac{a_2}{a_1}$$

3.2.3 Summary of the universality of theoretical concentration cell electrode potentials. In summary of the aforementioned classification discussions, the potential difference between the two half-cells has a unified expression, namely:

$$E = E^* - \frac{RT}{nF}\log Q \tag{20}$$

The standard electrode potential of the concentration cell is typically denoted as E^*. Since the electrodes on both sides are the same, its value is zero. It is important to note that the above equation indicates that the electromotive force of the cell depends on the concentration, which results in a strong correlation between free energy and concentration. The calculation of the Q value uses the following equation:

$$aA + bB \leftrightarrow cC + dD \tag{21}$$

$$Q = \frac{[C]^c[D]^d}{[A]^a[B]^b} \tag{22}$$

Substituting eqn (22) into eqn (21), we have:

$$E = -\frac{RT}{nF}\log\frac{[C]^c[D]^d}{[A]^a[B]^b} \tag{23}$$

Furthermore, the mass transfer coefficient k_m describes the rate of ion transport at the electrode surface and is related to the diffusion coefficient D and the thickness of the diffusion layer δ:

$$k_m = \frac{D}{\delta} \tag{24}$$

Here, δ can be estimated based on convection-diffusion theory as $\delta = \sqrt{\frac{DL}{v}}$, where L is the size of the cell and v is the flow velocity.

According to eqn (24) and the expression for the limiting current density:

$$j = zFk_mC_{bulk}\left(1 - \frac{E}{E_{max}}\right) \tag{25}$$

where E_{max} is the maximum potential, which depends on the mass transfer limiting conditions.

Combining with the Tafel equation, we obtain:

$$E = \frac{RT}{nF}\ln\left(\frac{j}{zFk_mC_{bulk}}\right) \tag{26}$$

Substituting eqn (26) and the relationship for δ into the equation, we obtain the general form of the concentration cell:

$$E = \frac{RT}{nF}\ln\left(\frac{j}{zF\frac{D}{\sqrt{\frac{DL}{v}}}C_{bulk}}\right) = \frac{RT}{nF}\ln\left(\frac{j\sqrt{\frac{DL}{v}}}{zFDC_{bulk}}\right) = \frac{RT}{nF}\ln\left(\frac{j\sqrt{L}}{zFC_{bulk}\sqrt{vD}}\right) \tag{27}$$

This equation represents the relationship between the concentration electrode potential and the correlation coefficients of the actual battery system, which is extremely important for designing and optimizing the performance of practical devices from a top-down perspective.

3.3 New optimization perspectives for concentration cells

Based on the above definitions, we can re-examine the energy storage mechanism of the concentration cell from a new perspective. The working mechanism of the concentration cell essentially depends on the difference in ion activities on both sides, which, from a phenomenological perspective, is due to the differing ion mobility, that is, the differences arising from varying mass transfer capabilities. Therefore, it is possible to consider regulating ion mobility to further enhance the electromotive force.

To improve ion mobility, a good approach is to adjust the viscosity of the electrolyte. Therefore, we propose a battery model in which a more viscous solution is placed in the left chamber, while a lower-viscosity electrolyte containing energy-storage ions is stored in the right chamber. When a certain voltage is applied to the electrodes on both sides, the ions are driven by the electric field into the viscous solution. We approximate the ions as moving spheres, and the viscous force acting on them can be calculated using the Navier–Stokes equation as follows:

$$F = 6\pi\eta vR \tag{28}$$

In the equation, R is the ion radius, v is its velocity relative to the liquid, and η is the viscosity coefficient of the liquid. When an electric field of intensity C is applied to an ion, the ion will accelerate under the influence of the electric field until it balances with the frictional resistance, at which point the ion will move at this limiting velocity.

Therefore, the magnitude of the force applied by the electric field is $|Z_i|eC$, where Z_i is the charge quantity and e is the elementary charge. When the limiting velocity is reached, the ion mobility u_i can be expressed as:

$$u_i = \frac{v}{C} = \frac{|Z_i|e}{6\pi\eta R} \tag{29}$$

By rearranging and transforming the formula, we can obtain the limiting velocity:

$$v = \frac{|Z_i|eC}{6\pi\eta R} \tag{30}$$

From eqn (25), it can be seen that when the viscosity of the solution is high, the ion diffusion rate significantly decreases to very low values. From both mesoscopic and macroscopic perspectives, the ions almost appear to be ''stopped'' in the electrolyte, effectively achieving a new form of ''embedding'' in the viscous liquid. This provides us with new insights for improving the electrolyte.

Therefore, when designing the electrolyte, one can consider incorporating viscosity modulation of the electrolyte as a synchronized variable in a system where dual-ion mutual diffusion occurs on both sides. By carefully designing and adjusting the viscosity levels of the electrolytes on both sides, it is also beneficial to create a disparity in ion diffusion rates, thereby modulating and optimizing the electromotive force of the concentration cell components from a new perspective.

3.4 Innovative design solutions for future concentration cells

The concentration cell, as an ''ancient yet young'' energy storage mode, has faced numerous challenges that hinder its rapid development, resulting in this storage mode being relegated to a ''neglected corner.'' However, this energy storage mode possesses significant application value. To facilitate the early large-scale application of such devices, we will provide a theoretical summary and discuss related issues from a renewed perspective, categorizing them accordingly.

3.4.1 Multifaceted collaborative design to enhance the electromotive force of concentration cells. The biggest challenge hindering these devices is that a single concentration cell can only produce a very small electromotive force, theoretically generating at most a few hundred millivolts. This extremely low potential significantly obstructs its widespread application in practical processes. Fortunately, we can ascertain from the general form of the electromotive force of concentration cells that the factors influencing the electromotive force are not related to the intrinsic parameters of the cell itself, but rather exhibit a strong correlation with the activity and mobility differences of the internal ions. Therefore, we can miniaturize the device and reference the highly integrated technology in the chip industry, integrating hundreds of millions or even billions of micro concentration cell components within a very small area.[25] By pre-designing the circuitry to connect the components in series and parallel, we can achieve a higher overall device electromotive force by linking the lower individual component electromotive forces, thereby laying a solid foundation for practical application.

In addition, we can also focus on the determinants of the electromotive force. This involves specifically addressing the low voltage issue of individual concentration cell components to effectively enhance the overall voltage of the final integrated device. From eqn (15), we can see that by increasing the ion concentration difference across the two sides of the cell and designing a bidirectional diffusion ionic system, we can achieve a synergistic enhancement of ion diffusion capabilities while optimizing the viscosity of the solutions on both sides, thereby effectively increasing the theoretical electromotive force.

3.4.2 Hardware optimization of concentration cell systems. Unfortunately, simply increasing the concentration difference to enhance the electromotive force of the components remains limited. This is explained by the general form of the diffusion flux-driving force equation we derived (eqn (2)). Increasing the concentration difference is essentially adjusting the linear diffusion coefficient in this equation, while the diffusion flux shows a linear relationship only with its degree of variation, resulting in a small change in potential increase. Therefore, we shift our focus to the exponential control coefficient in the equation. When we adjust the relevant parameters in the exponential control coefficient in synchrony, the change in diffusion flux will exhibit exponential growth.

For the adjustment of the exponential control coefficient, targeted modifications can be considered from two aspects. First, regarding the ion diffusion process, existing battery membranes primarily rely on size effects, meaning that diffusion through the membrane can occur freely as long as certain size conditions are met.[46,60] Clearly, such basic membranes struggle to meet the higher demands of concentration cells. For these types of devices, it is essential to develop ion channels similar to those in cell membranes that operate under reverse concentration gradients, facilitating the transport of ions against the concentration gradient after charging. Therefore, during the process of crossing such cell membrane-like battery separators, designing beneficial ''microstructures'' can help reduce the energy barriers required for ions to traverse the membrane, which would greatly benefit the exponential increase in ion diffusion flux. Additionally, beneficial external field adjustments can be made by designing different temperature gradients on the sides of the half-cells (referencing the area of melting) to promote high-flux ion diffusion.

3.4.3 Development of adaptive advanced theoretical simulations for concentration cells. With the rapid development of supercomputers, their computational power has increased dramatically. Therefore, applying advanced simulation methods to the device design of concentration cells and constructing battery optimization systems is of significant importance for achieving large-scale applications of such devices. By developing advanced adaptive simulation techniques, we can precisely control the internal circuit design of miniaturized devices, achieve accurate manufacturing of integrated components, and optimize specific device process flows such as the viscosity of the electrolyte and the selection of appropriate ion radii,

thereby greatly enhancing device performance. Through high-throughput computations combined with experimental data, we can develop machine learning models tailored to the specific properties of the electrolyte, and select descriptors that can accurately characterize battery behavior. Utilizing these machine learning models allows for precise assessments of battery lifecycle parameters and failure mechanisms, establishing safety warning strategies for the battery. These efforts will provide significant assistance for the practical application of concentration cells.

3.4.4 Construction of novel *in situ* testing equipment for interfacial reactions in concentration cells. *In situ* testing equipment plays an indispensable role in modern science, particularly in understanding reaction processes. By constructing novel *in situ* testing devices for interfacial reactions, we can establish a new physical framework for the relationship between ion diffusion parameters and changes in interfacial potential during the charge and discharge processes of concentration cells. This is especially important for illustrating the connections among these parameters and the final electromotive force of the battery. Additionally, developing advanced characterization paradigms based on an ''*in situ* + operating conditions'' model can reveal the mechanisms of electrochemical reactions under working conditions, enabling *in situ* characterization of the key dynamic changes in electrode structures and the electrode–electrolyte interface under simultaneous spatial and temporal conditions. By clarifying the microstructures and dynamic evolution patterns of the electrolyte and interface, we will gain deeper insights into the relevant mechanisms of concentration cells.

4. Conclusions

In summary, we start from the new theoretical perspective of the diffusion flux-driving force equation and propose a new degree of freedom for regulating ion mobility to improve the electromotive force (EMF) under working conditions, aiming to quickly address the inherent issues in the realization of concentration batteries. Subsequently, we provide a comprehensive summary of concentration batteries, analyzing the sources of their functional energy based on their operational characteristics. On this basis, we validate the practical applicability of various theoretical models through the derivation of their theoretical EMF and multiphysics simulations. Building on the new technical optimization perspective provided by this theory, we present a series of constructive recommendations for the future development of concentration battery devices, including the manufacture of highly integrated micro concentration batteries, the design of bidirectional diffusion ion systems, and the optimization of the viscosity of the electrolytes on both sides to achieve multi-faceted enhancements of the theoretical EMF of concentration batteries. To upgrade the hardware of the concentration battery systems, we can develop ''cell membrane-like'' battery separators targeting the exponential control coefficients and design different temperature zones to directionally adjust the diffusion flux of the charge-carrying ions. Furthermore, we need to develop adaptive advanced theoretical simulation methods to accurately assess the lifecycle parameters of the batteries and construct new *in situ* testing devices to reveal the key dynamic changes at the interface under operational conditions. By grounding our analysis in traditional theories and providing innovative technological solutions based on new engineering theoretical perspectives, this research paradigm will significantly accelerate the top-level structural optimization of new concentration batteries and have a significant impact on the future of new energy structures.

Author contributions

Z. S. Meng: conceptualization, data curation, formal analysis, investigation, methodology, project administration, resources, supervision, validation, and visualization; R. L. Zhang: software and roles; H. T. Sun: writing – original draft; J. C. Zhang: data curation; X. L. Gong: supervision; T. Deng: methodology; Z. Y. Du: investigation, data curation, formal analysis, investigation, and methodology.

Conflicts of interest

The authors declare no conflicts of interest.

Data availability

The data are available from the corresponding author upon reasonable request.

Acknowledgements

This work was financially supported by the Graduate Innovation Fund of Jilin University (Grant No. 2022177).

References

1 K. Wang, W. Xu, J. Li, H. Zheng, S. Sun, W. Song, Y. Song, Z. Ding, R. Zhang, Y. Sun, H. Zhang, J. Li and Z. Wang, Enhancing water droplet-based electricity generator by harnessing multiple-dielectric layers structure, *Nano Energy*, 2023, **111**, 108388.
2 X. Liu, H. Gao, J. E. Ward, X. Liu, B. Yin, T. Fu, J. Chen, D. R. Lovley and J. Yao, Power generation from ambient humidity using protein nanowires, *Nature*, 2020, **578**, 550–554.
3 A. S. Aricò, P. Bruce, B. Scrosati, J.-M. Tarascon and W. van Schalkwijk, Nanostructured materials for advanced energy conversion and storage devices, *Nat. Mater.*, 2005, **4**, 366–377.
4 S. Rahmstorf, The current climate, *Nature*, 2003, **421**, 699.
5 W. Xu, H. Zheng, Y. Liu, X. Zhou, C. Zhang, Y. Song, X. Deng, M. Leung, Z. Yang, R. X. Xu, Z. L. Wang,

X. C. Zeng and Z. Wang, A droplet-based electricity generator with high instantaneous power density, *Nature*, 2020, **578**, 392–396.
6 B. Dunn, H. Kamath and J.-M. Tarascon, Electrical Energy Storage for the Grid: A Battery of Choices, *Science*, 2011, **334**, 928–935.
7 Y. Li and Q. Cui, Carbon neutral growth from 2020 strategy and airline environmental inefficiency: A Network Range Adjusted Environmental Data Envelopment Analysis, *Appl. Energy*, 2017, **199**, 13–24.
8 J. M. Tarascon and M. Armand, Issues and challenges facing rechargeable lithium batteries, *Nature*, 2001, **414**, 359–367.
9 P. Simon and Y. Gogotsi, Materials for electrochemical capacitors, *Nat. Mater.*, 2008, **7**, 845–854.
10 V. Etacheri, R. Marom, R. Elazari, G. Salitra and D. Aurbach, Challenges in the development of advanced Li-ion batteries: a review, *Energy Environ. Sci.*, 2011, **4**, 3243–3262.
11 D. Larcher and J. M. Tarascon, Towards greener and more sustainable batteries for electrical energy storage, *Nat. Chem.*, 2015, **7**, 19–29.
12 K. Awasthi, V. Kulshrestha, R. Nathawat, N. K. Acharya, M. Singh, D. K. Avasthi and Y. K. Vijay, Conduction nature of conical pores in PET membrane, *Polym. Bull.*, 2006, **57**, 723–728.
13 Q. Zhang, Z. Hu, Z. Liu, J. Zhai and L. Jiang, Light-Gating Titania/Alumina Heterogeneous Nanochannels with Regulatable Ion Rectification Characteristic, *Adv. Funct. Mater.*, 2014, **24**, 424–431.
14 X. Meng, Z. Cai, Y. Zhang, X. Hu, Z. Xing, Z. Huang, Z. Huang, Y. Cui, T. Hu, M. Su, X. Liao, L. Zhang, F. Wang, Y. Song and Y. Chen, Bio-inspired vertebral design for scalable and flexible perovskite solar cells, *Nat. Commun.*, 2020, **11**, 3016.
15 Q. Zhang, Z. Liu, K. Wang and J. Zhai, Organic/Inorganic Hybrid Nanochannels Based on Polypyrrole-Embedded Alumina Nanopore Arrays: pH- and Light-Modulated Ion Transport, *Adv. Funct. Mater.*, 2015, **25**, 2091–2098.
16 Q. Li, Y. Qin, D. Cheng, M. Cheng, H. Zhao, L. Li, S. Qu, J. Tan and J. Ding, Moist-Electric Generator with Efficient Output and Scalable Integration Based on Carbonized Polymer Dot and Liquid Metal Active Electrode, *Adv. Funct. Mater.*, 2023, **33**, 2211013.
17 J. Gao, W. Guo, D. Feng, H. Wang, D. Zhao and L. Jiang, High-Performance Ionic Diode Membrane for Salinity Gradient Power Generation, *J. Am. Chem. Soc.*, 2014, **136**, 12265–12272.
18 Y. Huang, H. Cheng, C. Yang, P. Zhang, Q. Liao, H. Yao, G. Shi and L. Qu, Interface-mediated hygroelectric generator with an output voltage approaching 1.5 volts, *Nat. Commun.*, 2018, **9**, 4166.
19 Y. Jia, Q. Jiang, H. Sun, P. Liu, D. Hu, Y. Pei, W. Liu, X. Crispin, S. Fabiano, Y. Ma and Y. Cao, Wearable Thermoelectric Materials and Devices for Self-Powered Electronic Systems, *Adv. Mater.*, 2021, **33**, 2102990.
20 Q. Zhang, Z. Liu and J. Zhai, Photocurrent generation in a light-harvesting system with multifunctional artificial nanochannels, *Chem. Commun.*, 2015, **51**, 12286–12289.
21 K. C. Catania, Electric eels use high-voltage to track fast-moving prey, *Nat. Commun.*, 2015, **6**, 8638.
22 D. Shen, W. W. Duley, P. Peng, M. Xiao, J. Feng, L. Liu, G. Zou and Y. N. Zhou, Moisture-Enabled Electricity Generation: From Physics and Materials to Self-Powered Applications, *Adv. Mater.*, 2020, **32**, 2003722.
23 G. Xue, Y. Xu, T. Ding, J. Li, J. Yin, W. Fei, Y. Cao, J. Yu, L. Yuan, L. Gong, J. Chen, S. Deng, J. Zhou and W. Guo, Water-evaporation-induced electricity with nanostructured carbon materials, *Nat. Nanotechnol.*, 2017, **12**, 317–321.
24 X. Xiao, Y. Mei, Z. Ge, Y. Xu, Y. Huang, W. Deng, G. Zou, H. Hou and X. Ji, Electric-Eel-Type Bi-Ionic Gradient Battery, *ACS Appl. Mater. Interfaces*, 2023, **15**, 52641–52650.
25 D. P. Sheehan, A Self-Charging Concentration Cell: Theory, Batteries, *Batteries (Basel)*, 2023, **9**, 372.
26 J. Sun, X. Pu, M. Liu, A. Yu, C. Du, J. Zhai, W. Hu and Z. L. Wang, Self-Healable, Stretchable, Transparent Triboelectric Nanogenerators as Soft Power Sources, *ACS Nano*, 2018, **12**, 6147–6155.
27 H. Wang, T. He, X. Hao, Y. Huang, H. Yao, F. Liu, H. Cheng and L. Qu, Moisture adsorption-desorption full cycle power generation, *Nat. Commun.*, 2022, **13**, 2524.
28 J. Xu and D. A. Lavan, Designing artificial cells to harness the biological ion concentration gradient, *Nat. Nanotechnol.*, 2008, **3**, 666–670.
29 J. Xu, F. J. Sigworth and D. A. LaVan, Synthetic Protocells to Mimic and Test Cell Function, *Adv. Mater.*, 2010, **22**, 120–127.
30 T. Cai, L. Lan, B. Peng, C. Zhang, S. Dai, C. Zhang, J. Ping and Y. Ying, Bilayer Wood Membrane with Aligned Ion Nanochannels for Spontaneous Moist-Electric Generation, *Nano Lett.*, 2022, **22**, 6476–6483.
31 S. A. Hashemi, S. Ramakrishna and A. G. Aberle, Recent progress in flexible–wearable solar cells for self-powered electronic devices, *Energy Environ. Sci.*, 2020, **13**, 685–743.
32 M. He, W. Du, Y. Feng, S. Li, W. Wang, X. Zhang, A. Yu, L. Wan and J. Zhai, Flexible and stretchable triboelectric nanogenerator fabric for biomechanical energy harvesting and self-powered dual-mode human motion monitoring, *Nano Energy*, 2021, **86**, 106058.
33 H. Wang, Z. Rao, Y. Liu, L. Shan, T. Guo, H. Chen and R. Wang, A highly stretchable triboelectric nanogenerator with both stretch-insensitive sensing and stretch-sensitive sensing, *Nano Energy*, 2023, **107**, 108170.
34 Y. Xu, Z. Lin, W. Wei, Y. Hao, S. Liu, J. Ouyang and J. Chang, Recent Progress of Electrode Materials for Flexible Perovskite Solar Cells, *Nano-Micro Lett.*, 2022, **14**, 117.
35 D. Lin, Y. Liu and Y. Cui, Reviving the lithium metal anode for high-energy batteries, *Nat. Nanotechnol.*, 2017, **12**, 194–206.
36 M. F. L. De Volder, S. H. Tawfick, R. H. Baughman and A. J. Hart, Carbon Nanotubes: Present and Future Commercial Applications, *Science*, 2013, **339**, 535–539.
37 Z. Yang, J. Zhang, M. C. W. Kintner-Meyer, X. Lu, D. Choi, J. P. Lemmon and J. Liu, Electrochemical Energy Storage for Green Grid, *Chem. Rev.*, 2011, **111**, 3577–3613.

38 X.-B. Cheng, R. Zhang, C.-Z. Zhao and Q. Zhang, Toward Safe Lithium Metal Anode in Rechargeable Batteries: A Review, *Chem. Rev.*, 2017, **117**, 10403–10473.

39 C. Liu, F. Li, L.-P. Ma and H.-M. Cheng, Advanced Materials for Energy Storage, *Adv. Mater.*, 2010, **22**, E28–E62.

40 W. Lu, T. Ding, X. Wang, C. Zhang, T. Li, K. Zeng and G. W. Ho, Anion-cation heterostructured hydrogels for all-weather responsive electricity and water harvesting from atmospheric air, *Nano Energy*, 2022, **104**, 107892.

41 W. Zhang, F. Guo, H. Mi, Z.-S. Wu, C. Ji, C. Yang and J. Qiu, Kinetics-Boosted Effect Enabled by Zwitterionic Hydrogel Electrolyte for Highly Reversible Zinc Anode in Zinc-Ion Hybrid Micro-Supercapacitors, *Adv. Energy Mater.*, 2022, **12**, 2202219.

42 M. V. Reddy, G. V. Subba Rao and B. V. R. Chowdari, Metal Oxides and Oxysalts as Anode Materials for Li Ion Batteries, *Chem. Rev.*, 2013, **113**, 5364–5457.

43 J. Xue, T. Wu, Y. Dai and Y. Xia, Electrospinning and Electrospun Nanofibers: Methods, Materials, and Applications, *Chem. Rev.*, 2019, **119**, 5298–5415.

44 C. D. de Santana, W. G. R. Crampton, C. B. Dillman, R. G. Frederico, M. H. Sabaj, R. Covain, J. Ready, J. Zuanon, R. R. de Oliveira, R. N. Mendes-Júnior, D. A. Bastos, T. F. Teixeira, J. Mol, W. Ohara, N. Ce Castro, L. A. Peixoto, C. Nagamachi, L. Sousa, L. F. A. Montag, F. Ribeiro, J. C. Waddell, N. M. Piorsky, R. P. Vari and W. B. Wosiacki, Unexpected species diversity in electric eels with a description of the strongest living bioelectricity generator, *Nat. Commun.*, 2019, **10**, 4000.

45 T. B. H. Schroeder, A. Guha, A. Lamoureux, G. VanRenterghem, D. Sept, M. Shtein, J. Yang and M. Mayer, An electric-eel-inspired soft power source from stacked hydrogels, *Nature*, 2017, **552**, 214–218.

46 A. Guha, T. J. Kalkus, T. B. H. Schroeder, O. G. Willis, C. Rader, A. Ianiro and M. Mayer, Powering Electronic Devices from Salt Gradients in AA-Battery-Sized Stacks of Hydrogel-Infused Paper, *Adv. Mater.*, 2021, **33**, 2101757.

47 P. He, J. He, Z. Huo and D. Li, Microfluidics-based fabrication of flexible ionic hydrogel batteries inspired by electric eels, *Energy Storage Mater.*, 2022, **49**, 348–359.

48 Q.-C. Liu, J.-J. Xu, D. Xu and X.-B. Zhang, Flexible lithium–oxygen battery based on a recoverable cathode, *Nat. Commun.*, 2015, **6**, 7892.

49 Z. Zhang, S. Yang, P. Zhang, J. Zhang, G. Chen and X. Feng, Mechanically strong MXene/Kevlar nanofiber composite membranes as high-performance nanofluidic osmotic power generators, *Nat. Commun.*, 2019, **10**, 2920.

50 Z. Meng, Z. Xu, Z. Du, T. Deng, D. Wang, Y. Zeng, S. Yu, X. Hu and H. Tian, Prediction of future breakthroughs in materials synthesis and manufacturing techniques: a new perspective of synthesis dynamics theory, *Mater. Horiz.*, 2023, **10**, 5343–5353.

51 D. Zhao, J. Huang, Y. Zhong, K. Li, L. Zhang and J. Cai, High-Strength and High-Toughness Double-Cross-Linked Cellulose Hydrogels: A New Strategy Using Sequential Chemical and Physical Cross-Linking, *Adv. Funct. Mater.*, 2016, **26**, 6279–6287.

52 W. Guo, L. Cao, J. Xia, F.-Q. Nie, W. Ma, J. Xue, Y. Song, D. Zhu, Y. Wang and L. Jiang, Energy Harvesting with Single-Ion-Selective Nanopores: A Concentration-Gradient-Driven Nanofluidic Power Source, *Adv. Funct. Mater.*, 2010, **20**, 1339–1344.

53 H. Wang, Y. Sun, T. He, Y. Huang, H. Cheng, C. Li, D. Xie, P. Yang, Y. Zhang and L. Qu, Bilayer of polyelectrolyte films for spontaneous power generation in air up to an integrated 1000 V output, *Nat. Nanotechnol.*, 2021, **16**, 811–819.

54 L. Yang, F. Yang, X. Liu, K. Li, Y. Zhou, Y. Wang, T. Yu, M. Zhong, X. Xu, L. Zhang, W. Shen and D. Wei, A moisture-enabled fully printable power source inspired by electric eels, *Proc. Natl. Acad. Sci. U. S. A.*, 2021, **118**, e2023164118.

55 Y. Huang, H. Cheng, C. Yang, H. Yao, C. Li and L. Qu, All-region-applicable, continuous power supply of graphene oxide composite, *Energy Environ. Sci.*, 2019, **12**, 1848–1856.

56 P. Długołecki, A. Gambier, K. Nijmeijer and M. Wessling, Practical Potential of Reverse Electrodialysis As Process for Sustainable Energy Generation, *Environ. Sci. Technol.*, 2009, **43**, 6888–6894.

57 Z. Lin, Z. Meng, H. Miao, R. Wu, W. Qiu, N. Lin and X. Y. Liu, Biomimetic Salinity Power Generation Based on Silk Fibroin Ion-Exchange Membranes, *ACS Nano*, 2021, **15**, 5649–5660.

58 M. Wehner, R. L. Truby, D. J. Fitzgerald, B. Mosadegh, G. M. Whitesides, J. A. Lewis and R. J. Wood, An integrated design and fabrication strategy for entirely soft, autonomous robots, *Nature*, 2016, **536**, 451–455.

59 I. Must, F. Kaasik, I. Põldsalu, L. Mihkels, U. Johanson, A. Punning and A. Aabloo, Ionic and Capacitive Artificial Muscle for Biomimetic Soft Robotics, *Adv. Eng. Mater.*, 2015, **17**, 84–94.

60 C. Wang, E. Choi and J. Park, High-voltage nanofluidic energy generator based on ion-concentration-gradients mimicking electric eels, *Nano Energy*, 2018, **43**, 291–299.

